Theory of phase separation kinetics in polymer-liquid crystal systems

C. B. Muratov

Department of Mathematical Sciences,

New Jersey Institute of Technology, Newark, NJ 07102

Weinan E

Department of Mathematics, Princeton University, Princeton, NJ 08544

(Dated: December 21, 2001)

Abstract

We introduce a kinetic model describing the phase separation in the mixture of long rod-like molecules and long chain-like molecules. The model uses the angular distribution function for the orientations of the rods as a dynamical variable. The energetics is based on the non-local Onsager theory for the rods combined with a non-local extension of the Flory-Huggins theory. The kinetics explicitly takes into account the preferential diffusion along the rods. We computed the phase diagrams in this model and found a number of transitions leading to phase separation. We also performed numerical simulations of the phase separation kinetics and studied the resulting morphologies.

I. INTRODUCTION

Polymer-liquid crystal mixtures have attracted a great deal of attention lately[1]. From the viewpoint of applications, polymer matrix is used to stabilize liquid crystal displays[2]; polymeric composite materials have interesting mechanical and electrical properties which make them good candidates for a variety of applications[1,3,4]. Phase separation of such systems can be induced either through a thermal quench[3,4], or through polymerization[2].

In order to better control the properties of these materials, it is crucial to understand the morphology and dynamics of the phase separation process. Theoretical work on these problems are relatively scarce. Following earlier work of Shimada, Doi and Okano[5], Liu and Fredrickson derived TDGL (time dependent Ginzburg-Landau)-like equations using a dynamical mean field theory[6]. Their work illustrated the interplay between orientational order of the liquid crystals and the phase separation process[6,7]. But it also shares the same unpleasant feature that for a complex system such as the one considered here, a Ginzburg-Landau approach is bound to result in a large number of terms. This not only makes quantitative comparisons difficult but also seems to deviate from the original spirit of a Landau expansion.

Our approach is slightly more microscopic. We work at the level of kinetic theories such as Doi's equations[8]. We extend Doi's equation to the case of polymer-liquid crystal mixtures. The advantage of this approach is that we can build in directly the microscopic interaction potential between the molecules, which in the present paper is taken to be empirical, but in principle can be calculated directly from first principles. The disadvantage is that it is computationally more demanding, particularly since the interaction potential between rods involves a multi-fold integral over both translational (positional) and orientational (angle) degrees of freedom. This problem in the present paper is overcome by resorting to a gradient expansion which localizes the interaction with respect to position, but retains nonlocality in angle. Such a gradient expansion is considerably simpler than that of[6].

The main physical assumptions of our model can be summarized as follows. We are using a mean-field approach, so any fluctuation effects are not taken into consideration. We use simple phenomenological models of the excluded volume interaction. Specifically, to model the interaction between liquid crystal molecules we use the potential introduced by Priest and Straley[9–11]. For the kinetics, we assume that it is dominated by the translational and rotational diffusion of the liquid crystal molecules, thus ignoring all fluid effects. We neglect transversal diffusion of the liquid crystal molecules compared to their longitudinal diffusion. We also assume that the mixture of polymer and liquid crystal molecules is incompressible. In choosing the parameters of the model, we follow Doi[8].

First we derive the free energy functional that gives the free energy of the system in terms of the angular distribution function of the liquid crystal molecules. Next, we introduce a kinetic model that relates the fluxes of the liquid crystal molecules to the gradients of the liquid crystal chemical potential. The mobilities of the liquid crystal molecules obtained in this way are density- and orientation-dependent. We then introduce the gradient approximation that captures the dynamics of sufficiently slowly varying spatial distribution functions and use it in our simulations.

Our simulations show the importance of the interplay between liquid crystal ordering and phase separation, both energetically and kinetically. We find that at high polymer volume fractions, the system phase-separates into liquid crystal-rich droplets followed by ordering of the liquid crystal inside the droplets and leading to the formation of asymmetric droplets. At the same time, in the intermediate stages of this process the system evolves into connected bead-like structures similar to the ones observed in experiments[12]. We find that this morphology is a result of the kinetic rather than energetic effects. At equal volume fractions, the system evolves through the formation of a transient bead-like morphology into a stripe-like bicontinuous morphology, with the liquid crystal oriented along the stripes and the defects attached to the polymer-liquid crystal interfaces. At low polymer volume fractions we get distorted droplets of the polymer in the ordered liquid crystal matrix.

This paper is organized as follows. In the next section we discuss the energetic and kinetic aspects of our model. We will work with the orientation distribution function as the order parameter. We then discuss the phase diagrams in Section 3. Gradient expansion for the interaction potential is discussed in Section 4. Our simulation results are discussed in Section 5, followed by conclusions.

II. MODEL

In contrast to most previous works, we will be interested in a detailed description of the interaction of flexible polymers with the nematic liquid crystal molecules. As was first realized by Onsager, the fundamental quantity that describes the relevant degrees of freedom of the nematic is the distribution function $f_{\hat{\mathbf{n}}}$ of the nematic orientation $\hat{\mathbf{n}}$[8,13,14]. Onsager used this approach to explain the isotropic-nematic phase transition for lyotropic liquid crystals[13]. Priest and Straley used this approach to calculate the elastic moduli of the nematic solutions[9–11]. Doi used the distribution function $f_{\hat{\mathbf{n}}}$ to derive the kinetic model which describes the rotational diffusion of the solutions of rod-like molecules. The common feature of all these works is that they focus only on the distribution of the *orientation* of the nematic while neglecting the variation in its overall density. This is justified for the homogeneous solutions of the nematics. However, the situation becomes different when phase separation occurs and there exists an interplay between the nematic ordering and spatial inhomogeneity.

This interplay leads to a number of interesting phenomena. First, the free energy of the interaction between the liquid crystal and the polymer is going to be affected by the inhomogeneity of the polymer concentration and lead to the alignment between the orientation $\hat{\mathbf{n}}$ of the nematic molecules and the concentration gradients. Second, the orientational order should strongly affect the kinetics of phase segregation in a strongly entangled polymer-liquid crystal mixture. In the following, we will incorporate these effects into a model which describes both the energetics and the kinetics of the polymer-liquid crystal mixtures whose description is given in terms of the distribution function $f_{\hat{\mathbf{n}}}$.

A. Energetics

We start by writing the phenomenological free energy functional F of the polymer-liquid crystal system as a sum of three terms:

$$F = F_{lc} + F_{poly} + F_{int}, \tag{1}$$

where F_{lc} is the free energy functional for the liquid crystal subsystem, F_{poly} is the free energy of the flexible polymer subsystem, and F_{int} is the interaction free energy.

Let us look at the liquid crystal part first. We will use the non-local extension of the Onsager theory to describe the free energy due to the alignment of the nematic molecules in a spatially inhomogeneous system:

$$F_{lc} = \int d^d x d\hat{\mathbf{n}} \left(f_{\hat{\mathbf{n}}} \ln f_{\hat{\mathbf{n}}} + \frac{1}{2} \int d^d x' d\hat{\mathbf{n}}' B_{\hat{\mathbf{n}}\hat{\mathbf{n}}'}(x - x') f_{\hat{\mathbf{n}}}(x) f_{\hat{\mathbf{n}}'}(x') \right), \tag{2}$$

where d is the dimensionality of space, $\hat{\mathbf{n}}$ is the unit vector specifying the orientation of the liquid crystal molecule, $f_{\hat{\mathbf{n}}}(x)$ is the distribution function of the nematic orientations, and $B_{\hat{\mathbf{n}}\hat{\mathbf{n}}'}(x-x')$ is the pair interaction between the liquid crystal molecules (rods) with orientation $\hat{\mathbf{n}}$ and $\hat{\mathbf{n}}'$ located at x and x', respectively. If one considers only the excluded volume interaction, one can take B to be equal to 1 if the rods are intersecting and 0 otherwise[9–11,14]. In Eq. (2) the first term gives both the translational and the rotational entropy of the liquid crystal molecules, and the second term is the excluded volume interaction. Note that we chose the units in which $k_B T = 1$.

To describe the free energy of the inhomogeneous distribution of the polymer density, we use the Flory-Huggins theory with the square gradient term that penalizes spatial inhomogeneities

$$F_{poly} = \int d^d x \left(\frac{b^2 (\nabla \phi)^2}{2} + \frac{\phi}{N} \ln \phi + \chi_{poly} \phi^2 \right), \tag{3}$$

where ϕ is the volume fraction of the polymer, b is the coherence length, N is the polymerization index, and χ_{poly} is the Flory-Huggins parameter for the interaction between the polymer segments. In Eq. (3), the first term represents the conformational entropy of the chains, the second is their translational entropy, and the third is the interaction of the segments with each other. Note that one could use a more appropriate Lifshitz-DeGennes term $b^2(\nabla\phi)^2/\phi$ instead of the gradient square term in Eq. (3)[15,16]. This leads to essentially the same results, but complicates somewhat the numerical simulations.

Finally, we will model the contact interactions between the polymer and the liquid crystal by

$$F_{int} = \chi_{int} \int \phi \rho \, d^d x, \tag{4}$$

where χ_{int} is the polymer-liquid crystal interaction parameter,

$$\rho(x) = \int d\hat{\mathbf{n}} \int_{-L/2}^{L/2} dl f_{\hat{\mathbf{n}}}(x + \hat{\mathbf{n}} l) \tag{5}$$

is the segment number density of the liquid crystal molecules, and L is the number of segments in a liquid crystal molecule. Let us point out here the distinction between the distribution function $f_{\hat{\mathbf{n}}}(x)$, which gives the number of liquid crystal molecules with the center of mass in the volume element $d^d x$ and oriented within the solid angle $d\hat{\mathbf{n}}$, from the segment density $\rho(x)$. For long slender rods the latter is given by Eq. (5), since in this case the segment density of a *single* liquid crystal molecule centered at x' and oriented along $\hat{\mathbf{n}}$ can be taken as $\int_{-L/2}^{L/2} \delta(x - x' + \hat{\mathbf{n}}l)dl$, where $\delta(x)$ is the Dirac delta-function.

One should not forget the incompressibility condition which relates the values of $\phi(x)$ and $f_{\hat{\mathbf{n}}}(x)$ in space, so in fact $f_{\hat{\mathbf{n}}}(x)$ is the only relevant variable. In our case it takes the following form

$$\phi(x) + \rho(x) = 1. \tag{6}$$

This equation plays the role of the normalization condition for $f_{\hat{\mathbf{n}}}(x)$ in the spatially inhomogeneous system. Note that this incompressibility condition is *nonlocal* in the variable $f_{\hat{\mathbf{n}}}(x)$.

The set of equations above completely determines the free energy of the spatially inhomogeneous system in terms of the distribution function $f_{\hat{\mathbf{n}}}(x)$ of the nematic orientations and density. The physically relevant situation corresponds to $d = 3$. In this case the distribution function $f_{\hat{\mathbf{n}}}(x)$ depends on three spatial coordinates and two angles coming from the unit vector $\hat{\mathbf{n}}$. Furthermore, the interaction $B_{\hat{\mathbf{n}}\hat{\mathbf{n}}'}(x - x')$ is non-local in both the positions and the angular variables. Thus, using this distribution function in the simulations is a formidable challenge. For this reason, in the following we will work with systems constrained to two dimensions ($d = 2$). In this case $B_{\hat{\mathbf{n}}\hat{\mathbf{n}}'}(x - x')$ can be written explicitly as

$$B_{\hat{\mathbf{n}}\hat{\mathbf{n}}'}(x - x') = \begin{cases} 1, & x - x', \in ABCD \\ 0, & x - x', \notin ABCD \end{cases} \tag{7}$$

where $ABCD$ is the rhombus with the sides of length L, where L is the length of the liquid crystal molecules, parallel to $\hat{\mathbf{n}}$ and $\hat{\mathbf{n}}'$, respectively, whose center is at the origin (see Fig. 1). The distribution function $f_{\hat{\mathbf{n}}}(x)$, in turn, depends only on two spatial and one angular variable. Let us emphasize, however, that we are not trying to model two-dimensional nematics here. It is well-known that the fluctuation effects destroy nematic ordering in two dimensions, so our mean-field approach is not appropriate for these systems[17]. Nevertheless, we believe that on the level of the mean-field theory the restriction to two dimensions should capture well some qualitative features of the physically relevant three-dimensional system.

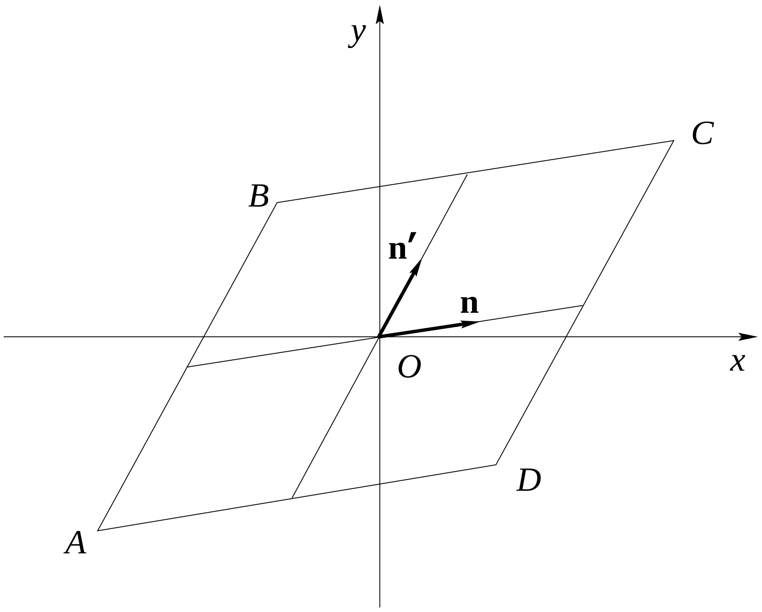

FIG. 1: Interaction potential geometry.

B. Kinetics

Let us now turn to the kinetics of the phase separation in polymer-liquid crystal systems. Since we are interested in phase separation, we need to study slow relaxation processes that lead to the segregation of phases. In polymer-liquid crystal systems these should be governed primarily by the translational diffusion of polymer and liquid crystal molecules and the rotational diffusion of the liquid crystal[8].

Let us look at the translational diffusion first. In a strongly entangled mixture of liquid crystal and polymer molecules the long rod-like liquid crystal molecules can move only in the direction of their orientation. In other words, only the longitudinal diffusion of the liquid crystal with the diffusion coefficient $D_{||}$ is allowed while the transversal diffusion is almost completely suppressed ($D_{\perp} = 0$)[8]. If we were dealing with the liquid crystal in a polymer matrix whose kinetics were driven by the gradient of the liquid crystal part of the chemical potential, the flux $\mathbf{j}_{\hat{\mathbf{n}}}$ of the liquid crystal molecules with the orientation vector $\hat{\mathbf{n}}$ would be

$$\mathbf{j}_{\hat{\mathbf{n}}} = -D_{||} f_{\hat{\mathbf{n}}} (\hat{\mathbf{n}} \otimes \hat{\mathbf{n}}) \nabla \mu_{lc}, \tag{8}$$

where $\mu_{lc} = \delta F / \delta f_{\hat{\mathbf{n}}}$, and we took into account that the flux is proportional to the density $f_{\hat{\mathbf{n}}}$. Observe that in Eq. (8) the flux is strongly coupled to the orientation distribution of the liquid crystal molecules. Similarly, if we were dealing with the polymer in a liquid crystal matrix, we would write the polymer flux $\mathbf{j}_\phi$ as

$$\mathbf{j}_\phi = -D_\phi \phi \nabla \mu_\phi, \tag{9}$$

where $\mu_\phi = \delta F/\delta\phi$ with $f_{\hat{\mathbf{n}}}$ fixed, and the dependence of the mobility on ϕ is taken into account. Note that if one assumes Rouse dynamics for flexible polymers and simple viscous drag for the liquid crystal, one gets the following estimates for the dependence of the diffusion coefficients on the parameters[8]:

$$D_\phi \sim 1, \quad D_{||} \sim L^{-1}, \tag{10}$$

where we measure time in the units in which the viscous drag coefficient of a single polymer segment (monomer) is of order 1.

In an incompressible mixture of the polymer and liquid crystal the fluxes $\mathbf{j}_{\hat{\mathbf{n}}}$ and $\mathbf{j}_\phi$ are no longer independent, but satisfy:

$$\nabla \cdot \left(\mathbf{j}_\phi + \int d\hat{\mathbf{n}} \int_{-L/2}^{L/2} \mathbf{j}_{\hat{\mathbf{n}}}(x + \hat{\mathbf{n}}l) dl \right) = 0. \tag{11}$$

In writing this equation we again took into account that the mass flux of the liquid crystal segments depends nonlocally on the liquid crystal flux $\mathbf{j}_{\hat{\mathbf{n}}}(x)$ and neglected the contributions from the rotational diffusion, which are small in the entangled mixture.

A proper way to introduce incompressibility to the kinetics would be to introduce a Lagrange multiplier (a scalar field) into the free energy and solve for one of the fluxes[18]. In the context of polymer-liquid crystal systems, in which there is a significant dependence of the mobilities on the concentrations of the species, this turns out to lead to a complicated elliptic problem. To overcome this difficulty, we will assume that $D_{||} \ll D_\phi/L$, so the kinetics is limited by the liquid crystal component. In this case the flux $\mathbf{j}_{\hat{\mathbf{n}}}$ must satisfy Eq. (8) in which instead of μ_{lc} one should take the chemical potential $\mu_{\hat{\mathbf{n}}}(x)$ of the system with the incompressibility constraint:

$$\begin{aligned} \mu_{\hat{\mathbf{n}}}(x) = \int d\hat{\mathbf{n}}' \int_{-L/2}^{L/2} dl \int_{-L/2}^{L/2} dl' \left\{ -b^2 \Delta f_{\hat{\mathbf{n}}'}(x + \hat{\mathbf{n}}'l' - \hat{\mathbf{n}}l) - 2\chi f_{\hat{\mathbf{n}}'}(x + \hat{\mathbf{n}}'l' - \hat{\mathbf{n}}l) \right\} \\ - \frac{1}{N} \int_{-L/2}^{L/2} dl \ln \left(1 - \int d\hat{\mathbf{n}}' \int_{-L/2}^{L/2} dl' f'_{\hat{\mathbf{n}}}(x + \hat{\mathbf{n}}'l' - \hat{\mathbf{n}}l) \right) \\ + \ln f_{\hat{\mathbf{n}}}(x) + \int d\hat{\mathbf{n}}' dx' B_{\hat{\mathbf{n}}\hat{\mathbf{n}}'}(x - x') f_{\hat{\mathbf{n}}'}(x'), \end{aligned} \tag{12}$$

where

$$\chi = \chi_{int} - \chi_{poly}. \tag{13}$$

This equation, however, does not take into account the slowing down of the dynamics at low volume fractions of the polymer. To account for it, we will use a standard approach and introduce a density-dependent diffusion coefficient $D(\phi)$ instead of $D_{||}$[16]. Thus, the flux of the liquid crystal molecules in our model has the form

$$\mathbf{j}_{\hat{\mathbf{n}}} = -D(\phi) f_{\hat{\mathbf{n}}} (\hat{\mathbf{n}} \otimes \hat{\mathbf{n}}) \nabla \mu_{\hat{\mathbf{n}}}, \quad D(\phi) = \frac{D_{||} D_\phi \phi}{L D_{||} + D_\phi \phi}. \tag{14}$$

So far, we were dealing with the translational diffusion of the polymer and the liquid crystal, and the effect of incompressibility. Let us now turn to the rotational diffusion of the liquid crystal. In a highly entangled mixture the coefficient of the rotational diffusion has the following dependence on the parameters[8]

$$D_r \sim \frac{a^2}{L^5}, \tag{15}$$

where a is the entanglement length which we will assume to be of order 1, that is, comparable to the monomer size, in our model. The rotational diffusion produces an extra flux $\mathbf{j}^r_{\hat{\mathbf{n}}}$ in the configuration space of $f_{\hat{\mathbf{n}}}$. In our model, we will ignore the effects of the tube dilations and will simply write this flux as

$$\mathbf{j}^r_{\hat{\mathbf{n}}} = -D_r f_{\hat{\mathbf{n}}} \nabla_{\hat{\mathbf{n}}} \mu_{\hat{\mathbf{n}}}. \tag{16}$$

Here $\nabla_{\hat{\mathbf{n}}}$ is the gradient in the space of orientations.

Summarizing all the results above, we are now able to write the continuity equation which gives a closed evolution equation for $f_{\hat{\mathbf{n}}}$ in the course of the phase separation

$$\frac{\partial f_{\hat{\mathbf{n}}}}{\partial t} + \nabla \cdot \mathbf{j}_{\hat{\mathbf{n}}} + \nabla_{\hat{\mathbf{n}}} \cdot \mathbf{j}^r_{\hat{\mathbf{n}}} = 0. \tag{17}$$

III. PHASE DIAGRAMS

We calculated the phase diagrams for our system for a set of values of N and L. These phase diagrams are presented in Figs. 2 – 7. In all these figures the solid lines are the lines of phase coexistence, the dashed lines are the spinodal and the nematic transition lines, and the dotted lines show the microphase separation transition (for the explanation see below).

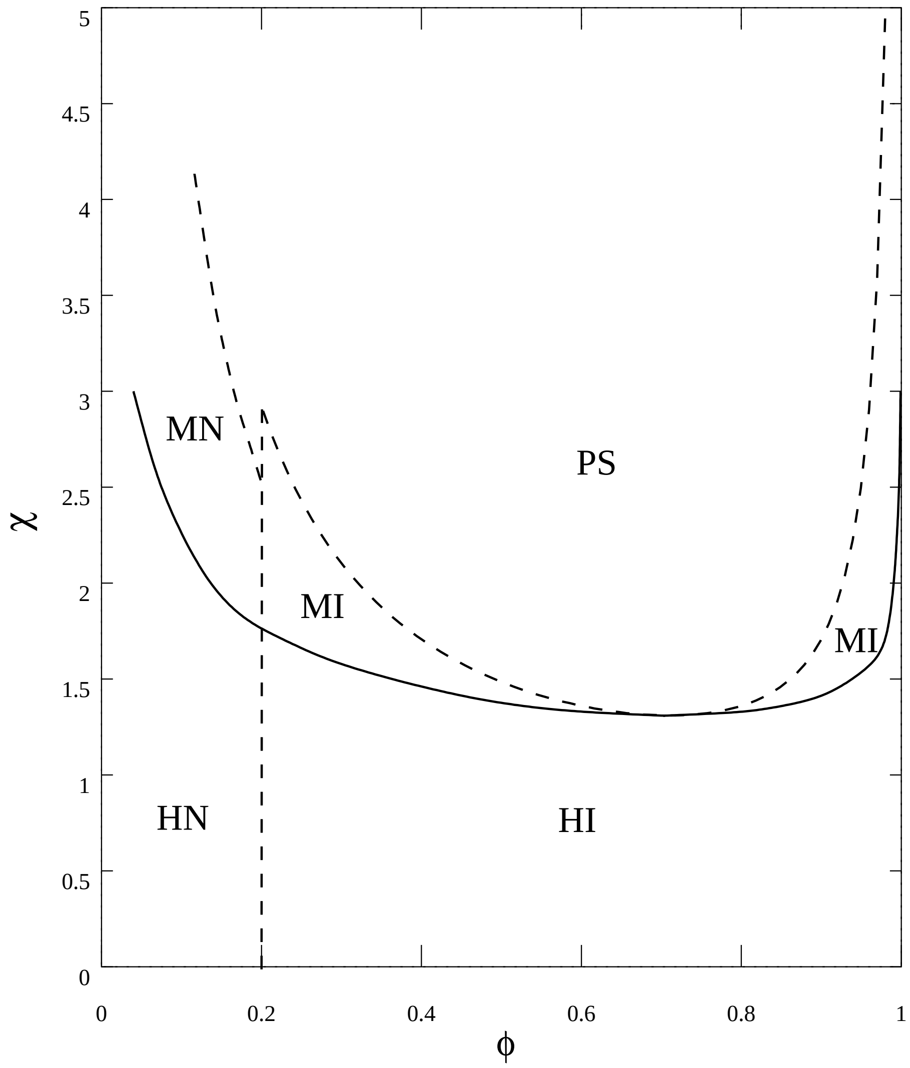

FIG. 2: Phase diagram for $L = 6$ and $N = 1$.

There are a number of regions in the phase diagrams separated by these lines which can be distinguished. Below the coexistence lines and to the right of the nematic transition the system in equilibrium is in the homogeneous isotropic state (HI). To the left from the isotropic-nematic transition line and below the coexistence line the equilibrium phase is homogeneous nematic (HN). Above the coexistence line and below the spinodal lines the homogeneous state of the system is isotropic metastable (MI) to the right of the isotropic-nematic transition line or nematic metastable (MN) to the left of this line. At long times these homogeneous metastable states will phase separate into polymer-rich isotropic and liquid crystal-rich nematic droplets via nucleation. Above the spinodal lines the homogeneous state becomes unstable and results in the spinodal decomposition and phase separation (PS).

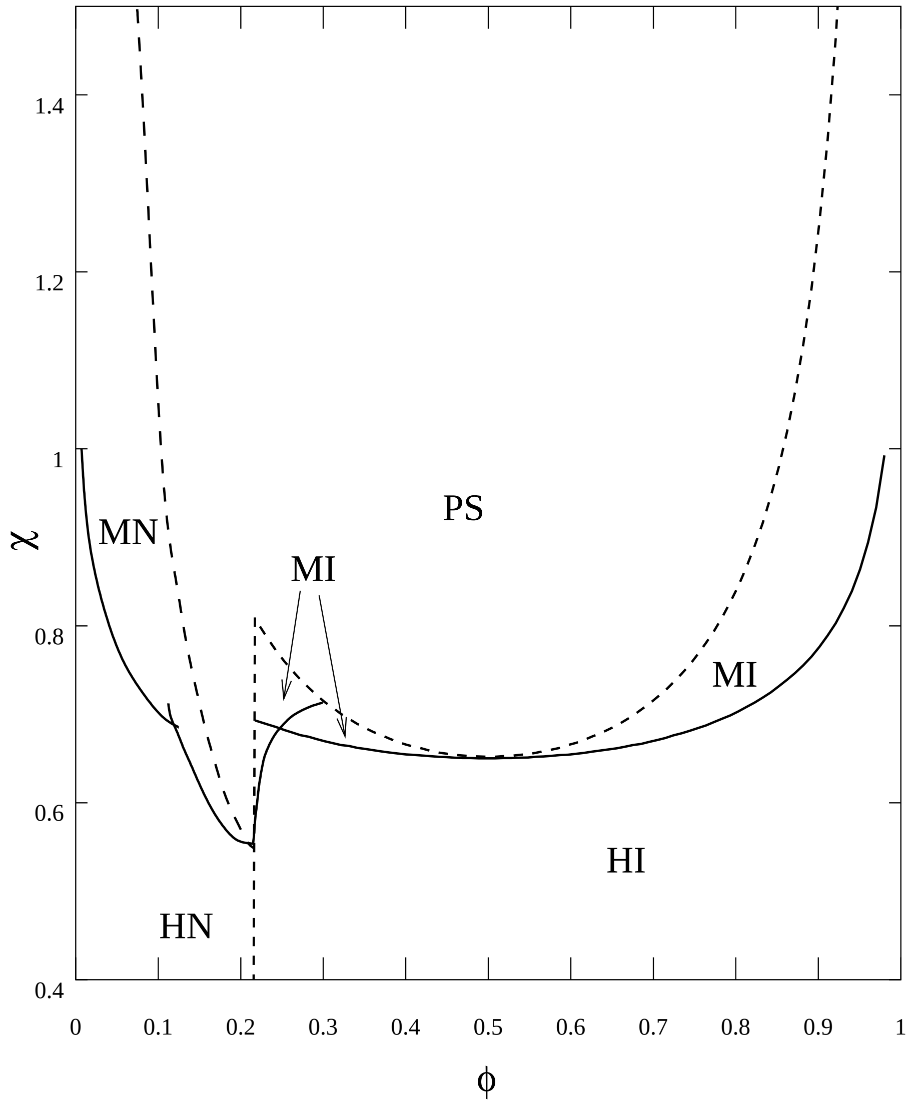

FIG. 3: Phase diagram for $L = 6$ and $N = 6$.

A. Nematic transition

We first look at the energetics of the homogeneous system. The free energy per unit volume of the homogeneous system is given by

$$\frac{F_{hom}}{V} = \frac{1}{N}\left(1 - L\int d\hat{\mathbf{n}} f_n\right)\ln\left(1 - L\int d\hat{\mathbf{n}} f_n\right) + \int d\hat{\mathbf{n}} f_{\hat{\mathbf{n}}}\ln f_{\hat{\mathbf{n}}}$$
$$+\frac{1}{2}\int d\hat{\mathbf{n}} d\hat{\mathbf{n}}'\beta(\hat{\mathbf{n}},\hat{\mathbf{n}}') f_{\hat{\mathbf{n}}} f_{\hat{\mathbf{n}}'} + \chi L\int d\hat{\mathbf{n}} f_n\left(1 - L\int d\hat{\mathbf{n}}' f_{\hat{\mathbf{n}}'}\right), \tag{18}$$

where

$$\beta(\hat{\mathbf{n}},\hat{\mathbf{n}}') = L^2|\hat{\mathbf{n}}\times\hat{\mathbf{n}}'| \tag{19}$$

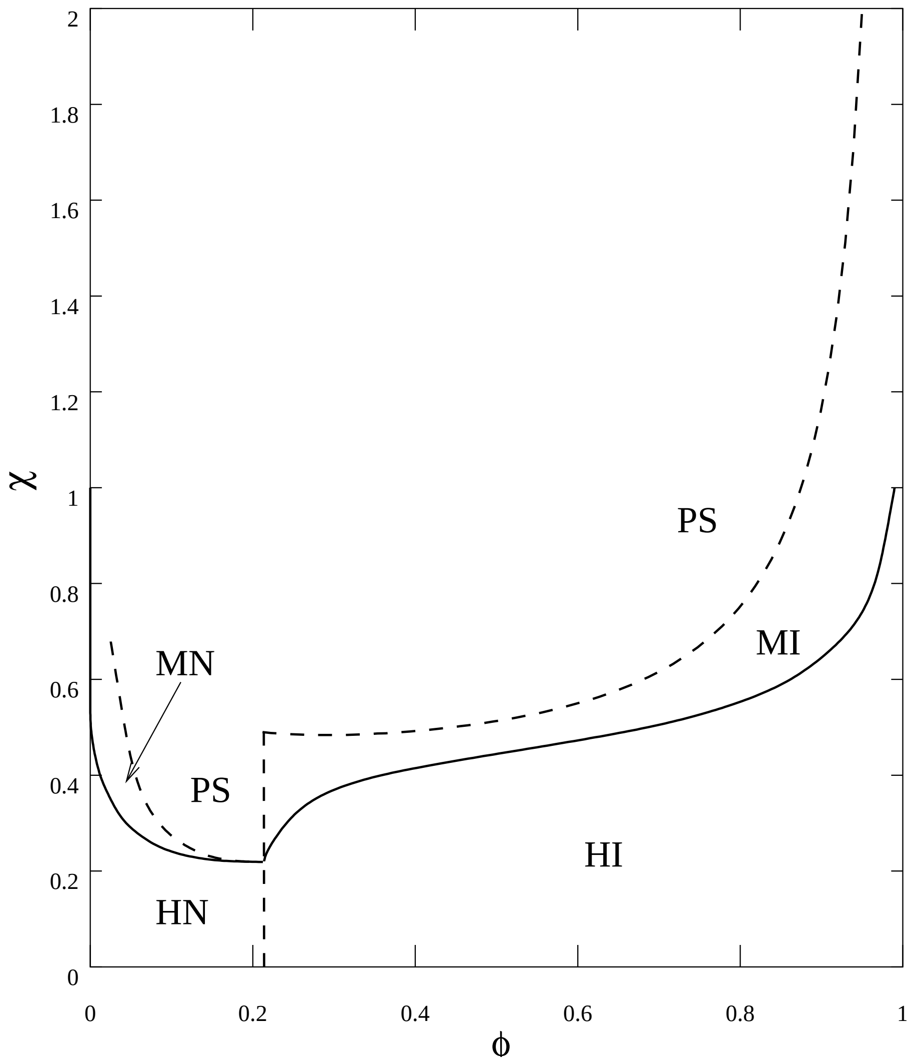

FIG. 4: Phase diagram for $L = 6$ and $N = 36$.

is the second virial coefficient which is obtained from Eq. (7) by integration over x and x' (it is just the area of the rhombus $ABCD$ in Fig. 1).

The free energy in Eq. (18) is then minimized numerically by discretizing the dependence of $f_{\hat{\mathbf{n}}}$ on $\hat{\mathbf{n}}$ for a given value of ϕ subject to the condition in Eq. (6). Depending on the value of ϕ, the equilibrium distribution function is either a constant corresponding to the isotropic phase, or a single-peaked function corresponding to the nematic phase. Since our system is two-dimensional, the isotropic-nematic transition is second-order (more precisely, the bifurcation of the free energy minimizers at the isotropic-nematic transition point is a supercritical pitchfork). Figure 8 shows the plot of the order parameter s defined in two

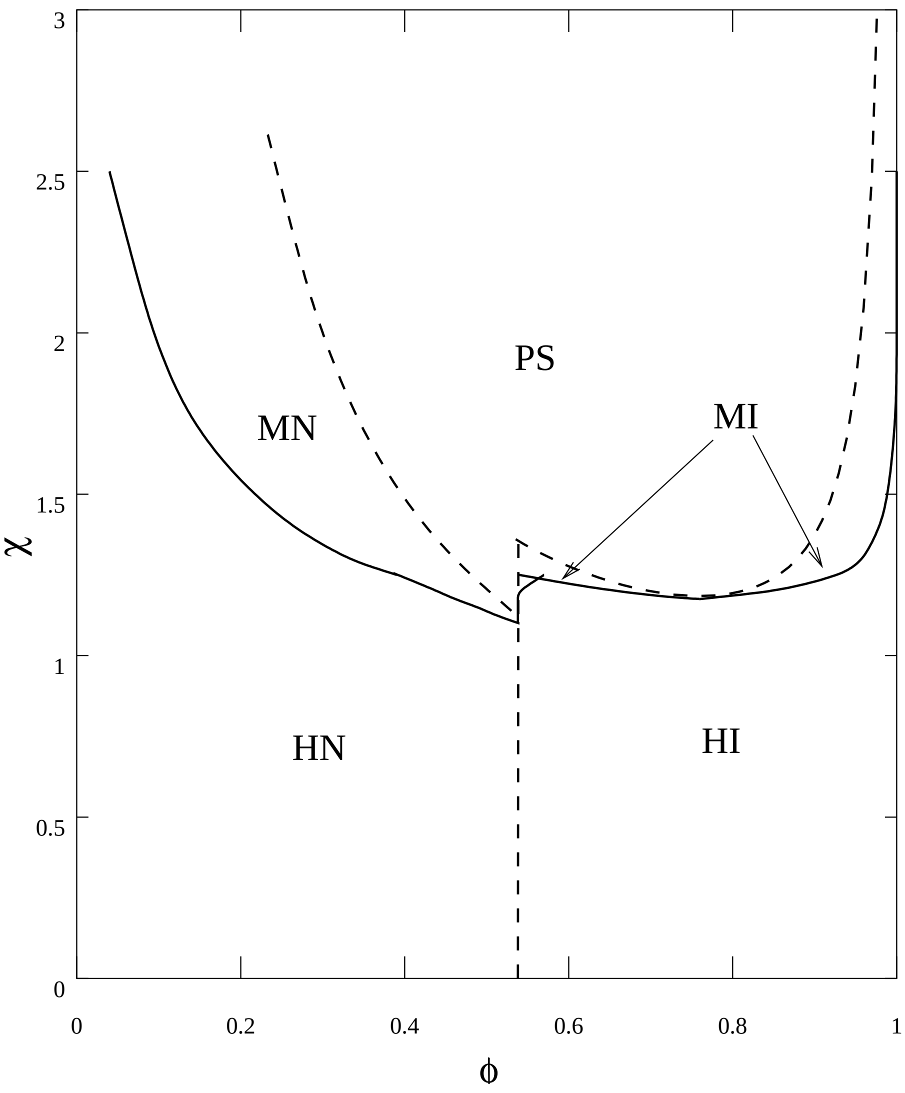

FIG. 5: Phase diagram for $L = 10$ and $N = 1$.

dimensions as

$$s = 2\langle\cos^2\rangle\theta - 1, \tag{20}$$

where averaging is with respect to the equilibrium distribution function $f^{eq}_{\hat{\mathbf{n}}}$, as functions of ϕ for different values of L. The nematic transition point is located at $\phi = \phi_{IN}$ with

$$\phi_{IN} = 1 - \frac{1}{L|\beta_2|}, \tag{21}$$

where $\beta_2 = -0.212$ (see below). Note that in our system the isotropic-nematic transition exists only for $L \gtrsim 5$.

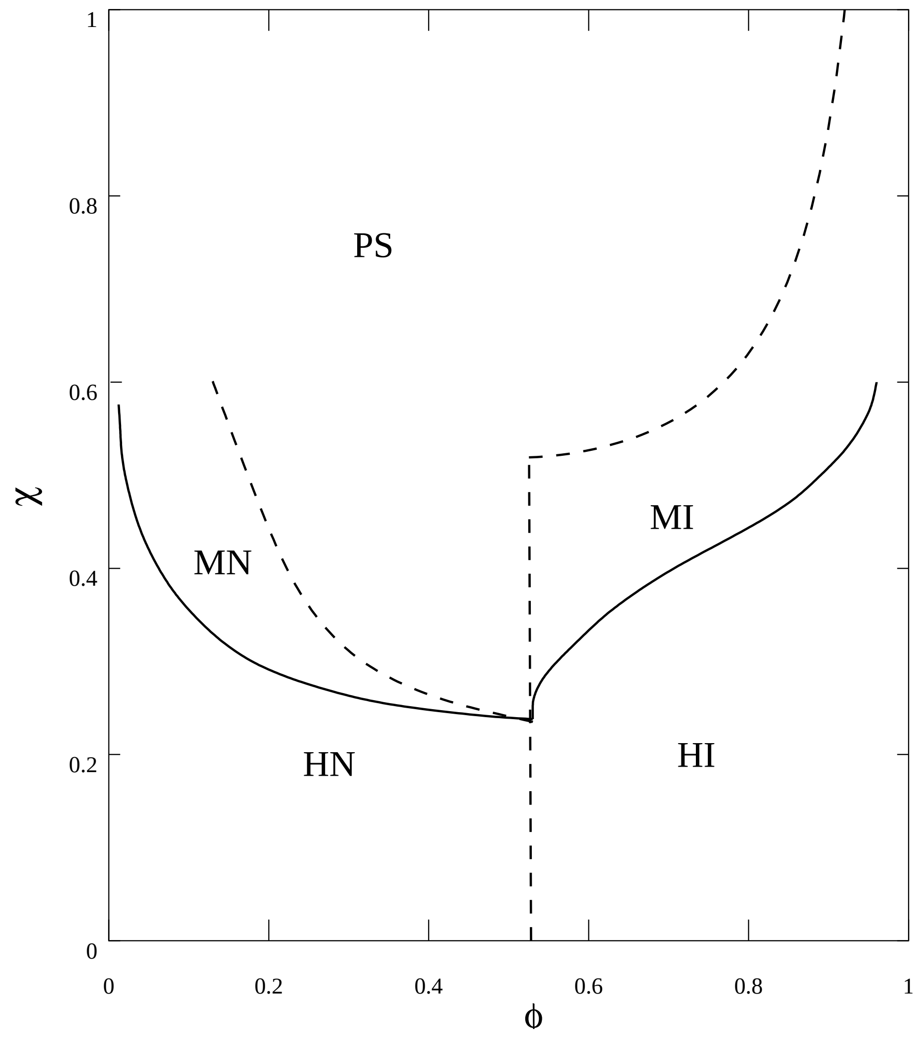

FIG. 6: Phase diagram for $L = 10$ and $N = 10$.

B. Phase coexistence and spinodal curves

If we substitute the obtained equilibrium distribution $f_{\hat{\mathbf{n}}}^{eq}$ in Eq. (18), we can calculate F_{hom} as a function of ϕ. The phase coexistence lines are then obtained from $F_{hom}^{eq}(\phi)$ using the double tangent construction.

Usually, there are only two coexisting phases when the system is in the metastable or phase separation regions. However, for some values of L and N there are regions of the parameter space where several coexisting phases can appear. The reason for this can be seen from Fig. 9 which shows the plot of the chemical potential μ as a function of ϕ for a particular set of parameters. Because of the isotropic-nematic transition the dependence $\mu(\phi)$ has a jump in the derivative $d\mu/d\phi$ at $\phi = \phi_{IN}$. As a result, there are several values

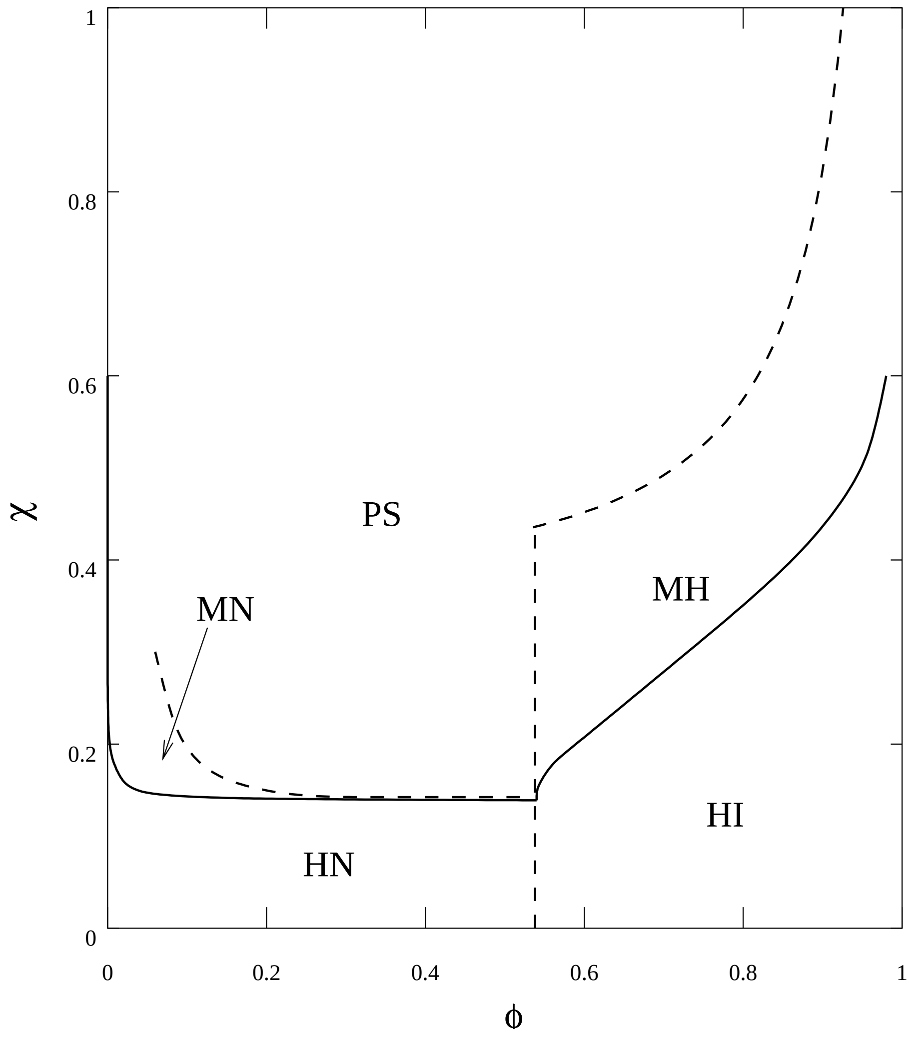

FIG. 7: Phase diagram for $L = 10$ and $N = 100$.

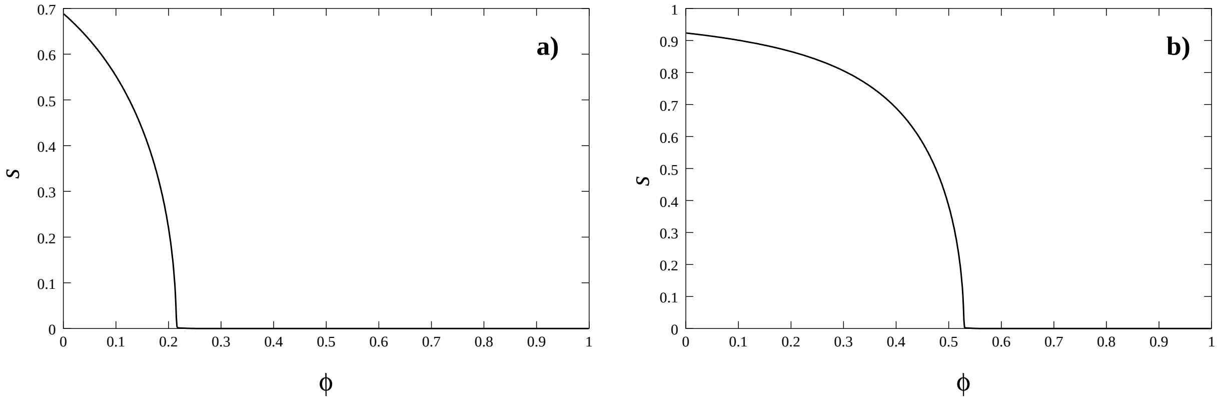

FIG. 8: Order parameter s as a function of the polymer concentration ϕ for $L = 6$ (a) and $L = 10$ (b).

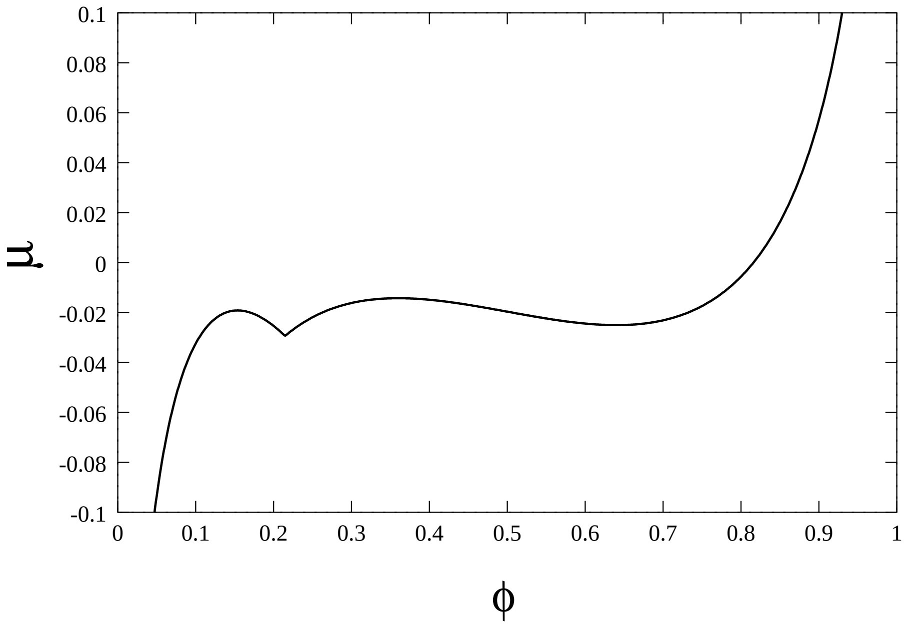

FIG. 9: Chemical potential μ as a function of the polymer density ϕ for $L = 6$, $N = 6$ and $\chi = 0.68$.

of μ and the corresponding values of ϕ for which the condition of phase equilibrium can be satisfied. This leads to a peculiarity in the energetics of the system for $L \simeq 6$.

The spinodal line is obtained by requiring non-negativity of the second variation $\delta^2 F_{hom}$. Let us first concentrate on the isotropic homogeneous state. Since this state possesses rotational invariance, the normal modes of the fluctuations will be $\delta f_{\hat{\mathbf{n}}} = e^{im\theta}$, where θ is the azimuthal angle and m is an even integer (recall that $f_{\hat{\mathbf{n}}}(x)$ does not depend on the sign of $\hat{\mathbf{n}}$). It is then not difficult to show from Eq. (18) that the second variation of the free energy with $\delta f_{\hat{\mathbf{n}}} = \sum_m \delta f_m e^{im\theta}$ relative to the homogeneous isotropic state is given by

$$\delta^2 F_{hom} = 2\pi^2 L^2 V \sum_m \left\{ \frac{1}{L(1-\phi)} + \delta_{m,0} \left(\frac{1}{N\phi} - 2\chi \right) + \beta_m \right\} |\delta f_m|^2, \tag{22}$$

where $\delta_{m,0}$ is the Kronecker delta,

$$\beta_m = \frac{1}{\pi} \int_0^\pi e^{im\theta} \sin\theta d\theta = \frac{2}{\pi(1-m^2)}. \tag{23}$$

Note that $\beta_0 > 0$ and $\beta_m < 0$ for $m \geq 2$.

From Eq. (22) one can see that the homogeneous isotropic state becomes unstable with respect to the $m = 0$ mode when

$$\chi \geq \chi_0 = \frac{1}{2} \left(\frac{1}{L(1-\phi)} + \frac{1}{N\phi} + \beta_0 \right), \tag{24}$$

which corresponds to the spinodal. Equation (22) also shows that at $\phi = \phi_{IN}$ given by Eq. (21) the homogeneous state becomes unstable with respect to the $m = 2$ mode. Numerically, we have $\beta_0 = 0.637$ and $\beta_2 = -0.212$.

When the system is in the homogeneous nematic state, one has to calculate the second variation $\delta^2 F_{hom}$ for the deviations $\delta f_{\hat{\mathbf{n}}}$ of $f_{\hat{\mathbf{n}}}$ from the equilibrium distribution $f^{eq}_{\hat{\mathbf{n}}}$ obtained in Sec. III A. This leads to the following expression for $\delta^2 F_{hom}$:

$$\delta^2 F_{hom} = \frac{V}{2}\left\{L^2\left(\frac{1}{\phi N} - 2\chi\right)\int \delta f_{\hat{\mathbf{n}}}\delta f_{\hat{\mathbf{n}}'} d\hat{\mathbf{n}} d\hat{\mathbf{n}}' + \int \frac{(\delta f_{\hat{\mathbf{n}}})^2}{f^{eq}_{\hat{\mathbf{n}}}} d\hat{\mathbf{n}} + \int \beta(\hat{\mathbf{n}}, \hat{\mathbf{n}}')\delta f_{\hat{\mathbf{n}}}\delta f_{\hat{\mathbf{n}}'} d\hat{\mathbf{n}} d\hat{\mathbf{n}}'.\right\} \tag{25}$$

This second variation defines a quadratic form and a corresponding generating Hermitian integral operator:

$$\delta^2 F_{hom} = \pi L^2 V \int \delta f_{\hat{\mathbf{n}}} \hat{L}_{hom} \delta f_{\hat{\mathbf{n}}} d\hat{\mathbf{n}}, \tag{26}$$

with

$$\hat{L}_{hom}\delta f_{\hat{\mathbf{n}}} = \frac{1}{2\pi}\left\{\frac{\delta f_{\hat{\mathbf{n}}}}{L^2 f^{eq}_{\hat{\mathbf{n}}}} + \int\left(\frac{1}{N\phi} - 2\chi + |\hat{\mathbf{n}} \times \hat{\mathbf{n}}'|\right)\delta f_{\hat{\mathbf{n}}'} d\hat{\mathbf{n}}'.\right\} \tag{27}$$

Discretizing $\delta f_{\hat{\mathbf{n}}}$ and diagonalizing $\hat{L}_{hom}$ numerically, we obtained the spinodal curves for the homogeneous nematic phase. They correspond to the values of χ as functions of $\phi < \phi_{IN}$ for which the lowest eigenvalue of the operator $\hat{L}_{hom}$ becomes negative.

C. Inhomogeneous fluctuations

Let us now consider the stability of the homogeneous state of the system with respect to arbitrary fluctuations (not necessarily homogeneous). In this case, according to Eq. (12), the second variation of the free energy will have the form

$$\begin{aligned}\delta^2 F = \frac{1}{2}\int d^2x d\hat{\mathbf{n}} d\hat{\mathbf{n}}' \int_{-L/2}^{L/2} dl \int_{-L/2}^{L/2} dl' \Big\{\left(-2\chi + \frac{1}{N\phi}\right)\delta f_{\hat{\mathbf{n}}}(x + \hat{\mathbf{n}}l)\delta f_{\hat{\mathbf{n}}'}(x + \hat{\mathbf{n}}'l') \\ + b^2 \nabla\delta f_{\hat{\mathbf{n}}}(x + \hat{\mathbf{n}}l)\cdot\nabla\delta f_{\hat{\mathbf{n}}'}(x + \hat{\mathbf{n}}'l') + \frac{2\pi L}{1-\phi}\delta f_{\hat{\mathbf{n}}}(x)\delta f_{\hat{\mathbf{n}}'}(x)\delta(\hat{\mathbf{n}} - \hat{\mathbf{n}}') \\ + \int dx' B(x - x'; \hat{\mathbf{n}}, \hat{\mathbf{n}}')\delta f_{\hat{\mathbf{n}}}(x)\delta f_{\hat{\mathbf{n}}'}(x')\Big\}.\end{aligned} \tag{28}$$

Because of the translational symmetry, the quadratic form in this equation can be partially diagonalized. Introducing $\delta f_{\hat{\mathbf{n}}}(x) = \sum_q \delta f_{q\hat{\mathbf{n}}} e^{iqx}$, after a straightforward but lengthy calculation, we get from Eq. (28)

$$\delta^2 F = \pi L^2 V \sum_q \int d\hat{\mathbf{n}} \delta f^*_{q\hat{\mathbf{n}}} \hat{L}_q \delta f_{q\hat{\mathbf{n}}}, \tag{29}$$

where the operator $\hat{L}_q$ is defined as

$$\begin{aligned} \hat{L}_q \delta f_{q\hat{\mathbf{n}}} = & \frac{1}{L(1-\phi)} \delta f_{q\hat{\mathbf{n}}} \\ & + \frac{1}{2\pi L^2} \int d\hat{\mathbf{n}}' \left(\frac{1}{N\phi} - 2\chi + b^2 q^2 + |\hat{\mathbf{n}} \times \hat{\mathbf{n}}'| \right) \frac{4 \sin\left[\frac{L}{2}(q\cdot\hat{\mathbf{n}})\right] \sin\left[\frac{L}{2}(q\cdot\hat{\mathbf{n}}')\right]}{(q\cdot\hat{\mathbf{n}})(q\cdot\hat{\mathbf{n}}')} \delta f_{q\hat{\mathbf{n}}'}. \end{aligned} \tag{30}$$

By discretizing $\delta f_{q\hat{\mathbf{n}}}$ in $\hat{\mathbf{n}}$ and diagonalizing the operator $\hat{L}_q$ from Eq. (30) numerically, we found that the instabilities always occur first with respect to the wave vector $q = 0$, so the only phase transitions that occur in our model are those considered above. An example of the spectrum λ_q of the operator $\hat{L}_q$ as a function of q for the set of parameters corresponding to the simulation in Fig. 14 is shown in Fig. 10.

IV. GRADIENT EXPANSION

The fully nonlocal chemical potential given by Eqs. (12) is very difficult to use in the simulations. For one thing, it gives very detailed information about the behavior of the system at short distances. If we are interested in the behavior of relatively long wave length modes, we can simplify this free energy functional by introducing a gradient expansion. This approach should be justified near the spinodal or the isotropic-nematic transition lines in the phase diagrams since the dominant instability modes in these cases are located at $q = 0$ (see Sec. III).

The gradient approximation for the chemical potential $\mu_{\hat{\mathbf{n}}}$ is obtained by assuming that $f_{\hat{\mathbf{n}}}$ is a slowly varying function of space and expanding the expressions like $f_{\hat{\mathbf{n}}}(x + \hat{\mathbf{n}}'l' - \hat{\mathbf{n}}l)$ in the Taylor series in l and l'. Using these approximations, after a lengthy but straightforward calculation we can write the expression for $\mu_{\hat{\mathbf{n}}}$ from Eq. (12) (up to a constant) as

$$\begin{aligned} \mu_{\hat{\mathbf{n}}} = \ln f_{\hat{\mathbf{n}}} - \frac{L}{N} \ln\phi + 2\chi L\phi + Lb^2\Delta\phi + \frac{L^3}{24N\phi^2}(\hat{\mathbf{n}}\cdot\nabla\phi)^2 + L^2 \int |\hat{\mathbf{n}} \times \hat{\mathbf{n}}'| f'_{\hat{\mathbf{n}}} d\hat{\mathbf{n}}' \\ + \frac{L^4}{24} \int \left(\frac{1}{N\phi} - 2\chi + |\hat{\mathbf{n}} \times \hat{\mathbf{n}}'| \right) \nabla \cdot [(\hat{\mathbf{n}}\otimes\hat{\mathbf{n}} + \hat{\mathbf{n}}'\otimes\hat{\mathbf{n}}')\nabla f_{\hat{\mathbf{n}}'}] d\hat{\mathbf{n}}', \end{aligned} \tag{31}$$

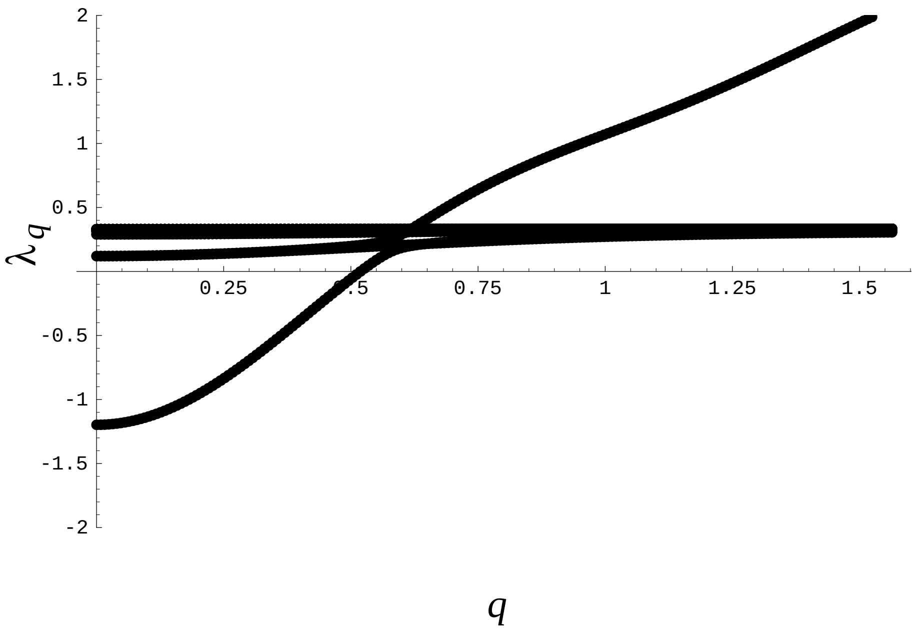

FIG. 10: The spectrum of the operator $\hat{L}_q$ from Eq. (30) as a function of the wave vector q at $N = 6, L = 10, b = 2, \phi = 0.5$ and $\chi = 1.25$.

where to the leading order in the gradient expansion

$$\phi(x) = 1 - L \int f_{\hat{\mathbf{n}}}(x) d\hat{\mathbf{n}}. \tag{32}$$

Note a term proportional to $(\hat{\mathbf{n}} \cdot \nabla\phi)^2$ in Eq. (31) which results in anchoring of the liquid crystal molecules perpendicularly to the direction of $\nabla\phi$. The evaluation of $\mu_{\hat{\mathbf{n}}}$ involves only the calculation of $f_{\hat{\mathbf{n}}}$ itself and the derivatives up to second of $f_{\hat{\mathbf{n}}}$. Thus, the problem associated with the non-locality in space of the original interaction kernel $B_{\hat{\mathbf{n}}\hat{\mathbf{n}}'}(x - x')$ has been eliminated. Equation (31) together with Eqs. (14), (16) (32) and (17) are a closed set of equations that determine the evolution of the distribution function $f_{\hat{\mathbf{n}}}$ from given initial conditions.

One still has to make sure that the obtained set of equations is well-posed, that is, there is no blowup of the arbitrarily short wavelength modes. In the case of the fully nonlocal theory this clearly should not be the case since the contributions of $B_{\hat{\mathbf{n}}\hat{\mathbf{n}}'}(x - x')$ and the polymer-liquid crystal interaction vanish for these modes. As a result, at short wave lengths the system should behave as a mixture of non-interacting polymer and liquid crystal molecules. However, we will see below that this is in general not the case for the reduced theory (Eq. (31)).

Let us see how the inhomogeneous fluctuations $\delta f_{q\hat{\mathbf{n}}}$ with the wave vector q affect the free energy for small deviations from the stable homogeneous state. For small $\delta f_{q\hat{\mathbf{n}}}$ the variation of the free energy $\delta^2 F$ will be given by Eq. (29), where $\hat{L}_q$ has to be replaced by $\hat{L}_q^g$ with

$$\begin{aligned} \hat{L}_q^g \delta f_{q\hat{\mathbf{n}}} = \hat{L}_{hom} \delta f_{q\hat{\mathbf{n}}} + \frac{b^2 q^2}{2\pi} \int \delta f_{q\hat{\mathbf{n}}'} d\hat{\mathbf{n}}' \\ -\frac{L^2}{48\pi} \int \left(\frac{1}{N\phi} - 2\chi + |\hat{\mathbf{n}} \times \hat{\mathbf{n}}'| \right) q^T (\hat{\mathbf{n}} \otimes \hat{\mathbf{n}} + \hat{\mathbf{n}}' \otimes \hat{\mathbf{n}}') q \delta f_{q\hat{\mathbf{n}}'} d\hat{\mathbf{n}}', \end{aligned} \tag{33}$$

and $\hat{L}_{hom}$ given by Eq. (27).

We still have to verify that the problem is well-posed since there is a possibility that the operator $\hat{L}_q^g$ has large negative eigenvalues for large enough q. This is in fact generally the case. In order to analyze the spectrum of the operator L_q^g for large q, we discretized this operator and diagonalized it numerically. The spectrum for a particular set of the parameters is presented in Fig. 11. From this figure one can see that for large enough q there is a branch of the spectrum with $\lambda_q < 0$, signifying an instability. On the other hand, in the region of interest in which $q \sim 1$ the spectrum of the operator $\hat{L}_q^g$ approximates well the spectrum of $\hat{L}_q$. Therefore, the negative sign of λ_q for large enough q is an artifact of the gradient expansion and is not associated with any physical behavior. It is simply a consequence of the fact that the gradient expansion breaks down for large enough q. To avoid this problem, one needs to introduce a short-range cutoff $q = q_{max}$, so that $\lambda_q > 0$ for all $q < q_{max}$. In practice, the cutoff is naturally introduced in the numerical implementations of the equations by choosing sufficiently coarse mesh size Δx, so that $q_{max} \geq \pi/\Delta x$.

V. SIMULATIONS OF THE KINETICS

We have performed the numerical simulations of our kinetic model based on the gradient expansion approximation (Sec. IV). The system was quenched into the regions of the phase diagram in which the homogeneous isotropic state becomes thermodynamically unstable. The governing equations were discretized both in time and the angular variable $\hat{\mathbf{n}}$, with periodic boundary conditions. We found that the discretization steps $\Delta x = 1.5$, $\Delta t = 0.1$, and $\Delta\theta = 0.26$ (for the azimuthal angle) were adequate for the parameters we used. The initial conditions were taken in the form of the isotropic uniform mixture with small random fluctuations. The model was then run up to sufficiently long times at which the dynamics of

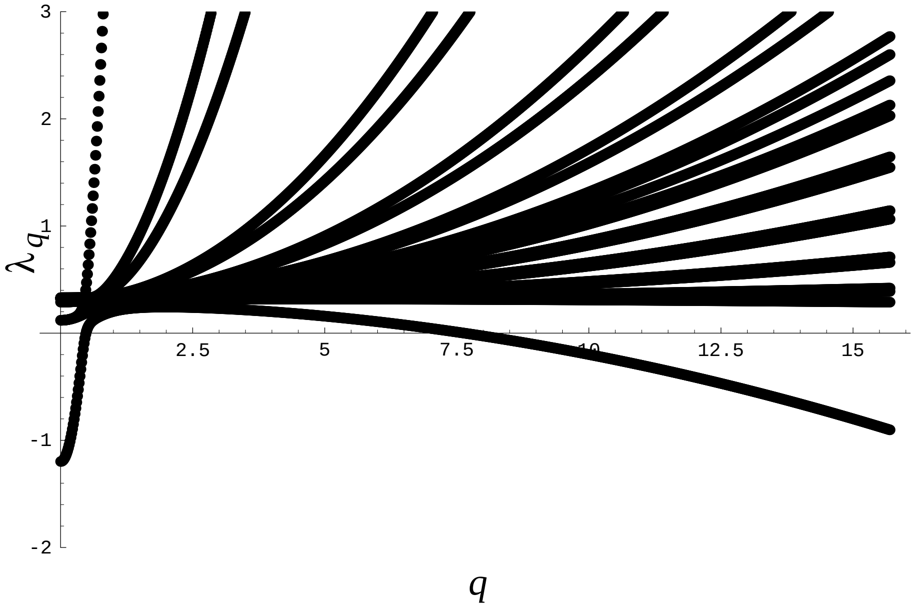

FIG. 11: The spectrum λ_q of the operator $\hat{L}_q^g$ from Eq. (33) for $b = 2$, $L = 6$, $N = 6$, $\chi = 1.25$, $\phi = 0.5$

the system becomes very slow. Note that the simulations of our model require a substantial amount of computational power since they involve the discretization not only in space, but also in $\hat{\mathbf{n}}$, with the couplings between all possible $\hat{\mathbf{n}}$'s (see Eq. (31)). For this reason, the code was optimized for running on an R10000 SGI Origin2000 supercomputer, also allowing for parallelization.

Before reporting our simulation results, let us say a few words about the choice of the parameters. In order for the simulations not to run into the regime in which the orientation distribution function $f_{\hat{\mathbf{n}}}$ is sharply peaked in the orientation space, we chose a modest value of $L = 6$. Since the system more easily undergoes the spinodal decomposition when $L \simeq N$, in the simulations we chose them to be equal. Note that the phase diagram of our system is most complex for these values of N and L (see Fig. 3). The ratio between the translational and rotational diffusion coefficients was chosen so as to reflect the effect of the entanglement. Thus the free parameters in our simulations are the volume fraction of the polymer ϕ and the polymer-liquid crystal interaction parameter χ.

In the first example we chose a polymer-rich mixture ($\phi = 0.7$). Figure 12 shows a sequence of snapshots of the state of the system at different times. The upper panels in each snapshot show the distribution of the polymer density with red corresponding to the pure polymer and blue to the liquid crystal, respectively. The lower panels in each snapshot show the magnitude of the order parameter at different points in space.

One can see three qualitatively different regimes. In the early stages of the phase separation (the first 5 snapshots in Fig. 12) a bead-like morphology is formed. After a period of linear growth of about 1000 time units the systems starts to form an interconnected network of liquid crystal-rich beads. For these times the rotational diffusion of the liquid crystal molecules is negligible, so the transport is dominated by the translational diffusion.

The formation of the beads is accompanied by a kinetic ordering of the liquid crystal in the polymer-rich regions (see the lower panels in Fig. 12). We would like to emphasize that this ordering is not related with the energetic nematic ordering which occurs in the later stages of the phase separation. What happens is, as the minority liquid crystal molecules move together into localized regions, the fastest molecules are those oriented perpendicularly to the gradient of the liquid crystal concentration. If the localized region in which the excess liquid crystal molecules accumulate is elongated, the molecules that are oriented *perpendicularly* to the axis of this elongated region move into this region first, leaving an excess of the molecules oriented in parallel with the axis of this region behind in the polymer-rich region.

This effect can be illustrated by Fig. 13. Figures 13(a) and 13(b) show the director field scaled by the order parameter, and the polymer density, respectively, at the moment when the kinetic ordering occurs. One can see from Fig. 13(a) that at the time of the picture the liquid crystal-rich regions (dark regions in Fig. 13(b)) are not ordered, while the polymer-rich regions (light regions in Fig. 13(b)) are strongly ordered.

This kinetic ordering in the polymer-rich regions becomes quite substantial, with the magnitude of the order parameter reaching ~ 0.5. Note that because the liquid crystal molecules in the polymer-rich regions are oriented perpendicularly to the gradient of the polymer concentration, the transport of these liquid crystal molecules into the liquid crystal-rich regions becomes *suppressed*. Indeed, since the rotational diffusion is negligible at this time scale, a liquid crystal molecule can only diffuse in the direction of its (fixed) orientation. Therefore, if the molecule is oriented perpendicularly to the direction of the gradient of the chemical potential, no motion will occur. This effect produces long-range correlations in the dynamics of the system, resulting in the formation of the network of beads.

After a time of order 1500 time units the second regime starts. The growth of the liquid crystal-rich regions is saturated and the droplets made of almost pure liquid crystal phase in the matrix of the almost pure polymer phase form. After that the characteristic time scale of the variations of the concentration dramatically decreases, substantially slowing down the dynamics. At this point the rotational diffusion of the liquid crystal molecules, which so far was negligible, becomes important and destroys the kinetic ordering produced in the first stage of the phase separation. The main driving mechanism for the dynamics becomes the curvature of the interfaces between the polymer and the liquid crystal-rich phases. Since the constraint imposed by the kinetic ordering of the liquid crystal now disappears, the network-like structure of the liquid crystal-rich phase breaks down.

At times of the order of 2000 time units the compact liquid crystal-rich droplets form, and the third and final stage of the dynamics begins. As the droplets are formed, the liquid crystal molecules inside start to order into the nematic phase, making the droplets a little elongated and producing point defects at the most curved portions of the interfaces. The anchoring effects produce a layer of the liquid crystal molecules oriented perpendicularly to the interfaces on the outside of the droplets and in parallel with the interfaces inside them. This can be seen in Figs. 13(c) and (d). The late stage dynamics is evaporation-condensation coarsening of these droplets. The defects do not seem to play any role in the dynamics here. Since the liquid crystal phase is the minority here, so the defects attached to different droplets do not interact.

In the second example the polymer volume fraction was chosen to be the same as that of the liquid crystal ($\phi = 0.5$). The results of the simulation are presented in Fig. 14. One can see that the three stages of the dynamics discussed above are still present, but with certain modifications. As in the previous simulation, the initial stage leads to the formation of an interconnected network of beads. However, because of the greater liquid crystal volume fraction, in the second stage the morphology does not break up into a droplet morphology, but rather develops into a bicontinuous stripe-like morphology. As the dynamics enters the third stage, the ordering of the liquid crystal in the direction of the stripes produces a global anisotropy in the system. The stripes then coarsen, but the overall global direction of the nematic ordering remains.

During coarsening, the stripes break up into droplets or coalesce. The point defects (blue spots in the sea of yellow in the order parameter pictures) that form in the second stage of the phase segregation remain attached to the points of high curvature of the interfaces. We do not see any substantial motion of the defects along the interfaces once the defects are attached. The annihilation of the defects occurs when portions of the interfaces containing them merge during coarsening.

In the third example, the polymer is the minority phase ($\phi = 0.2$). The results of the simulation are shown in Fig. 15. In this case we do not see the formation of the network structure or the kinetic ordering. As the droplets of the minority polymer-rich phase form, a nematic phase transition in the liquid crystal matrix occurs, with the droplets working as the initiators. The nematic ordering results in the formation of the point defects that quickly move to the droplet interfaces. Once again, we do not typically see the annihilation of the defects attached to the same droplet. Because of the defects, the interfaces become distorted, producing asymmetric droplets. These droplets once again coarsen via the evaporation-condensation mechanism. Here, however, we do see interaction between the defects attached to different droplets. These defects attract, pulling the droplets closer together. When the droplets come closer, the evaporation-condensation mechanism intensifies, so the smaller droplet disappears before the droplets come in contact. This process increases somewhat the speed of coarsening.

VI. CONCLUSION

In conclusion, we developed a model describing the phase separation in polymer-liquid crystal mixtures. This model uses the angular orientation distribution function as the dynamical variable and thus gives a detailed description of the diffusion of the liquid crystal molecules. Thus, our approach can be considered more microscopic than the TDGL approach of[6,7].

We found that the anisotropic transport due to the inability of the liquid crystal molecules to move perpendicularly to their axis produces kinetic ordering of these molecules in the early stages of the phase separation which is contrary to the ordering of the liquid crystal in the nematic phase. This leads to the formation of a transient connected bead-like morphology for low volume fractions of the liquid crystal. Similar morphologies are observed in experiments on polymer-stabilized liquid crystals[12].

The late stages of the phase separation are dominated by the dynamics of the interfaces and the coarsening of the morphology due to the evaporation-condensation mechanism. The nematic ordering of the liquid crystal in the droplets leads to their distortions and significant deviations from the circular shape. Also, point defects forming in the nematic attach to the interfaces. On the time scales we were able to run our simulations we did not see a significant effect of the defects on the motion of the interfaces.

The next step in our approach would be to perform simulations of the fully nonlocal model without resorting to the gradient expansion. Computationally, this is challenging because it would require evaluating multiple convolutions at each moment in time. We hope that this can be achieved with the use of the spectral methods in space. The extra computational cost associated with using Fast Fourier Transform may be compensated by the ability of choosing larger time steps. This should also allow to use the method of Lagrange multipliers to properly account for the incompressibility of the mixture.

ACKNOWLEDGMENTS

This work is supported in part by an Air Force grant F 49620-98-1-0256.

REFERENCES

[1] National Research Council Report, *Liquid Crystalline Polymers* (National Academy Press, Washington, D.C., 1990).

[2] G. P. Crawford and S. Zumer, *Liquid Crystals in Complex Geometries Formed by Polymer and Porous Networks* (Taylor and Fracis, London, 1996).

[3] J. H. Aubert and R. L. Clough, Polymer **26**, 2047 (1985).

[4] C. L. Jackson and M. T. Shaw, Polymer **31**, 1071 (1990).

[5] T. Shimada, M. Doi, and K. Okano, J. Chem. Phys. **88**, 7181 (1988).

[6] A. Liu and G. F. Fredrickson, Macromolecules **29**, 8000 (1996).

[7] A. M. Lapena, S. Glotzer, S. A. Langer, and A. Liu, Phys. Rev. E **60**, R29 (1999).

[8] M. Doi and S. F. Edwards, *The Theory of Polymer Dynamics* (Clarendon Press, New York, 1986).

[9] J. P. Straley, Mol. Cryst. Liq. Cryst **22**, 333 (1973).

[10] J. P. Straley, Mol. Cryst. Liq. Cryst **24**, 7 (1973).

[11] R. G. Priest, Phys. Rev. A **7**, 720 (1973).

[12] C. V. Rajaram, S. D. Hudson, and L. C. Chien, Chemistry of Materials **8**, 2451 (1996).

[13] L. Onsager, Ann. NY Acad. Sci. **51**, 627 (1949).

[14] A. Y. Grosberg and A. R. Khokhlov, *Statistical Physics of Macromolecules* (AIP Press, New York, 1994).

[15] I. M. Lifshitz, A. Y. Grosberg, and A. R. Khokhlov, Rev. Mod. Phys. **50**, 683 (1978).

[16] P. G. de Gennes, J. Chem. Phys. **72**, 4756 (1980).

[17] D. Forster, *Hydrodynamic fluctuations, broken symmetry, and correlation functions* (Addison-Wesley, Redwood City, CA, 1990).

[18] W. E and P. Palffy-Muhoray, Phys. Rev. E **55**, R3844 (1997).

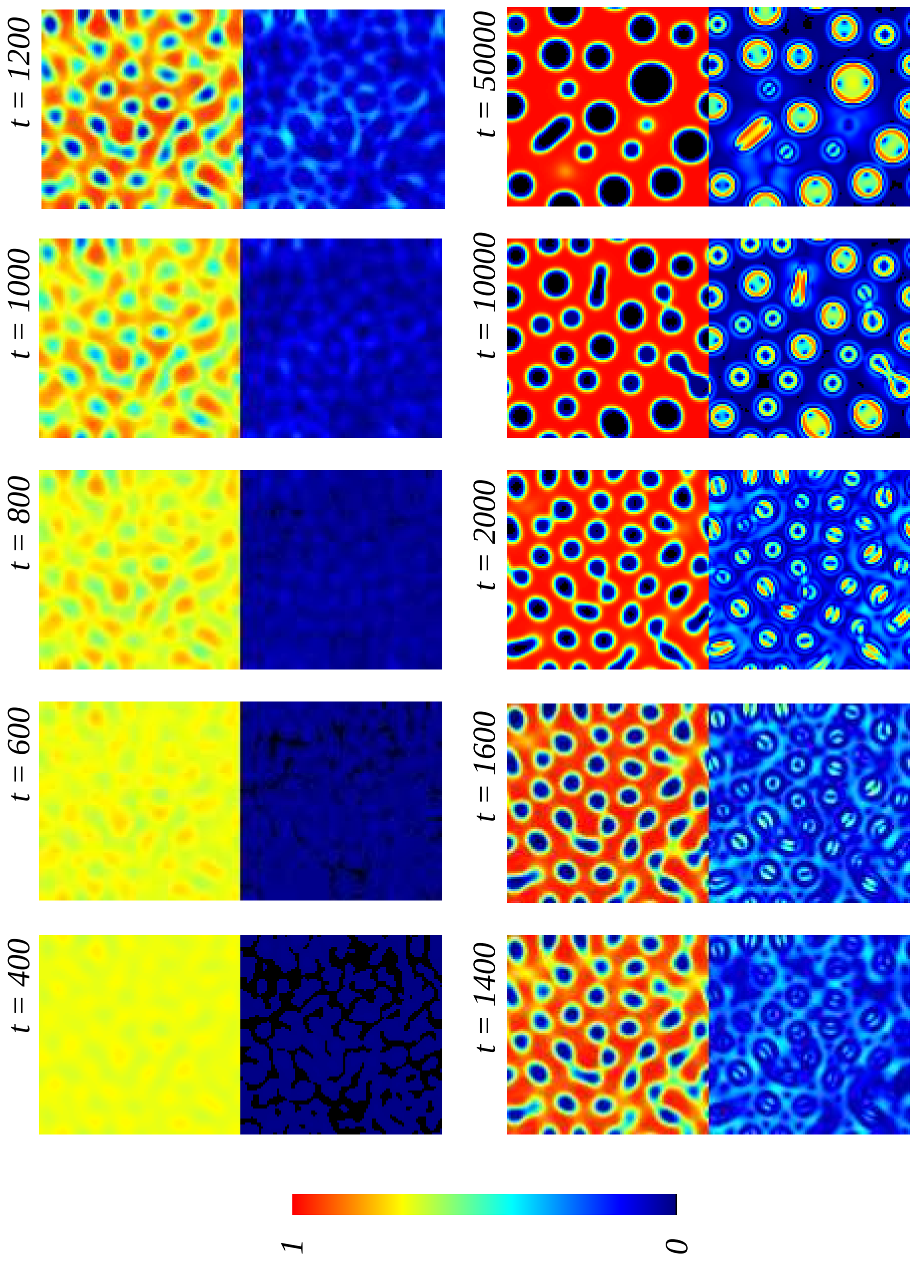

FIG. 12: Numerical simulations of the model for $L = 6$, $N = 6$, $\phi = 0.7$, $b = 2$, $\chi = 1.25$, $LD_{||} = 1$, $D_\phi = 0.1$, $D_r = 8.3 \times 10^{-4}$. The system is 150×150.

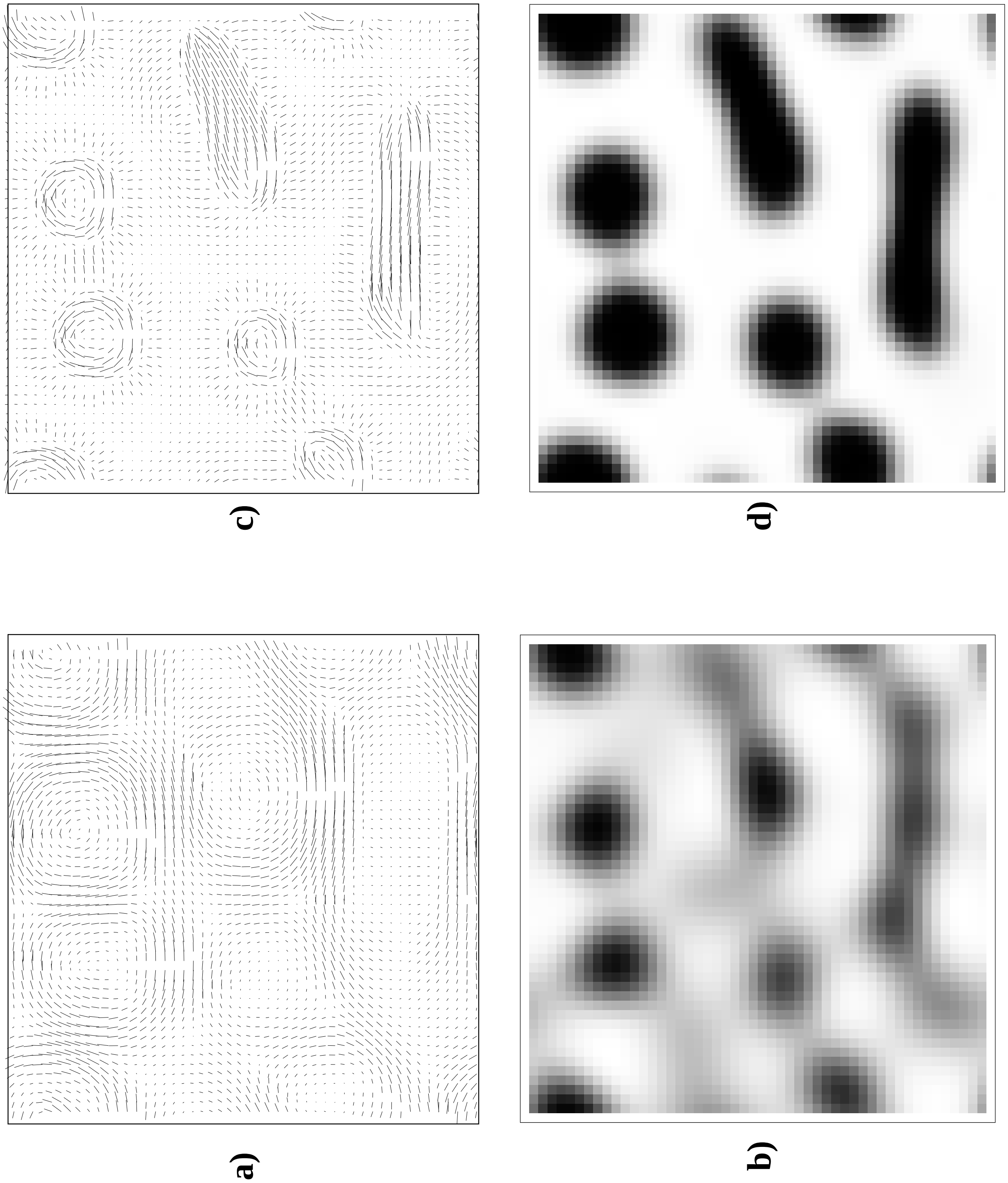

FIG. 13: The kinetic and energetic ordering of the liquid crystal: the distribution of the director scaled by the magnitude of the order parameter at $t = 1200$ (a), the distribution of the polymer density at $t = 1200$ with lighter regions corresponding to the polymer-rich regions (b), the distribution of the director scaled by the magnitude of the order parameter at $t = 2000$ (c), the distribution of the polymer density at $t = 2000$ with lighter regions corresponding to the polymer-rich regions (d). In all four panels the parameters of the simulation are those of Fig. 12. The system is 75×75.

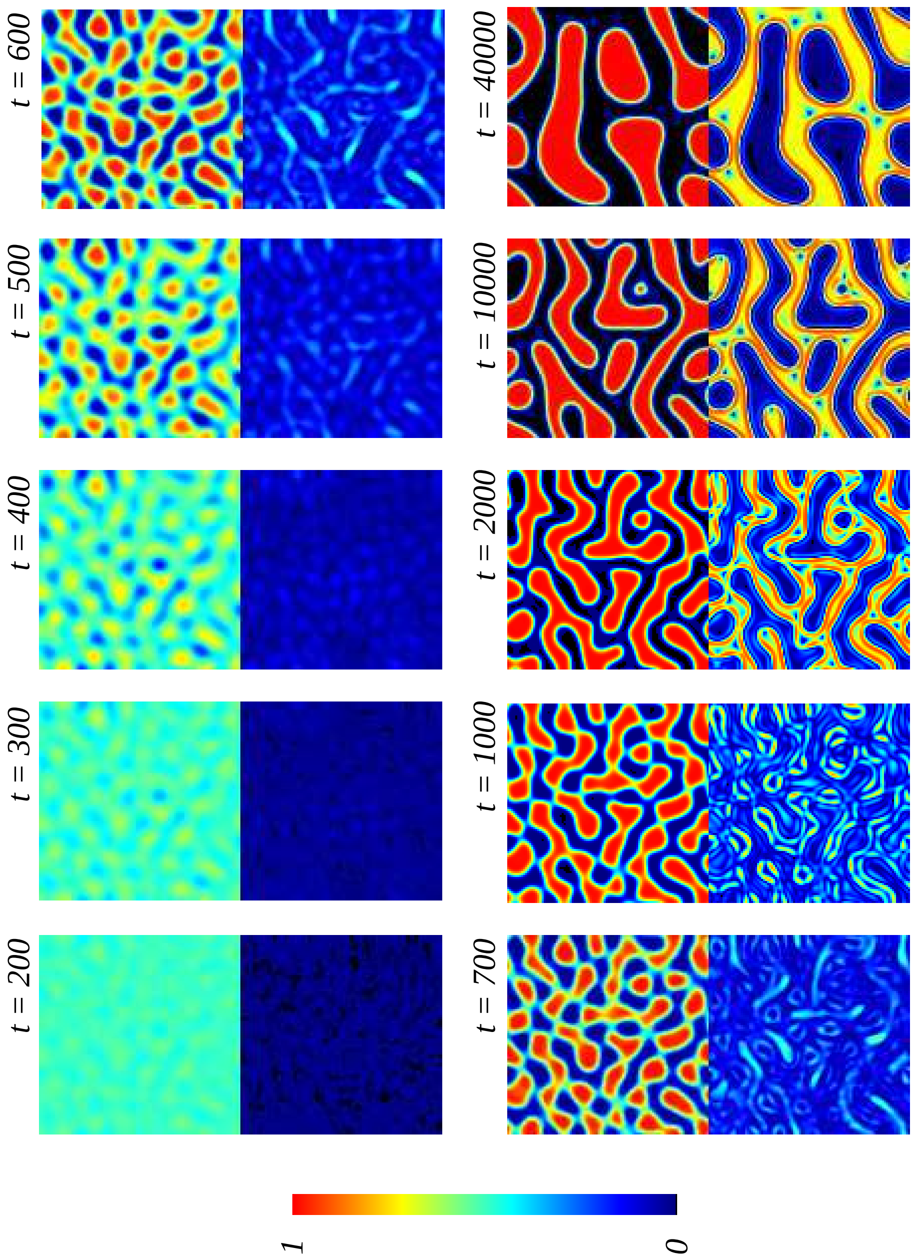

FIG. 14: Numerical simulations of the model for $L = 6$, $N = 6$, $\phi = 0.5$, $b = 2$, $\chi = 1.25$, $LD_{||} = 1$, $D_\phi = 0.1$, $D_r = 8.3 \times 10^{-4}$. The system is 150×150.

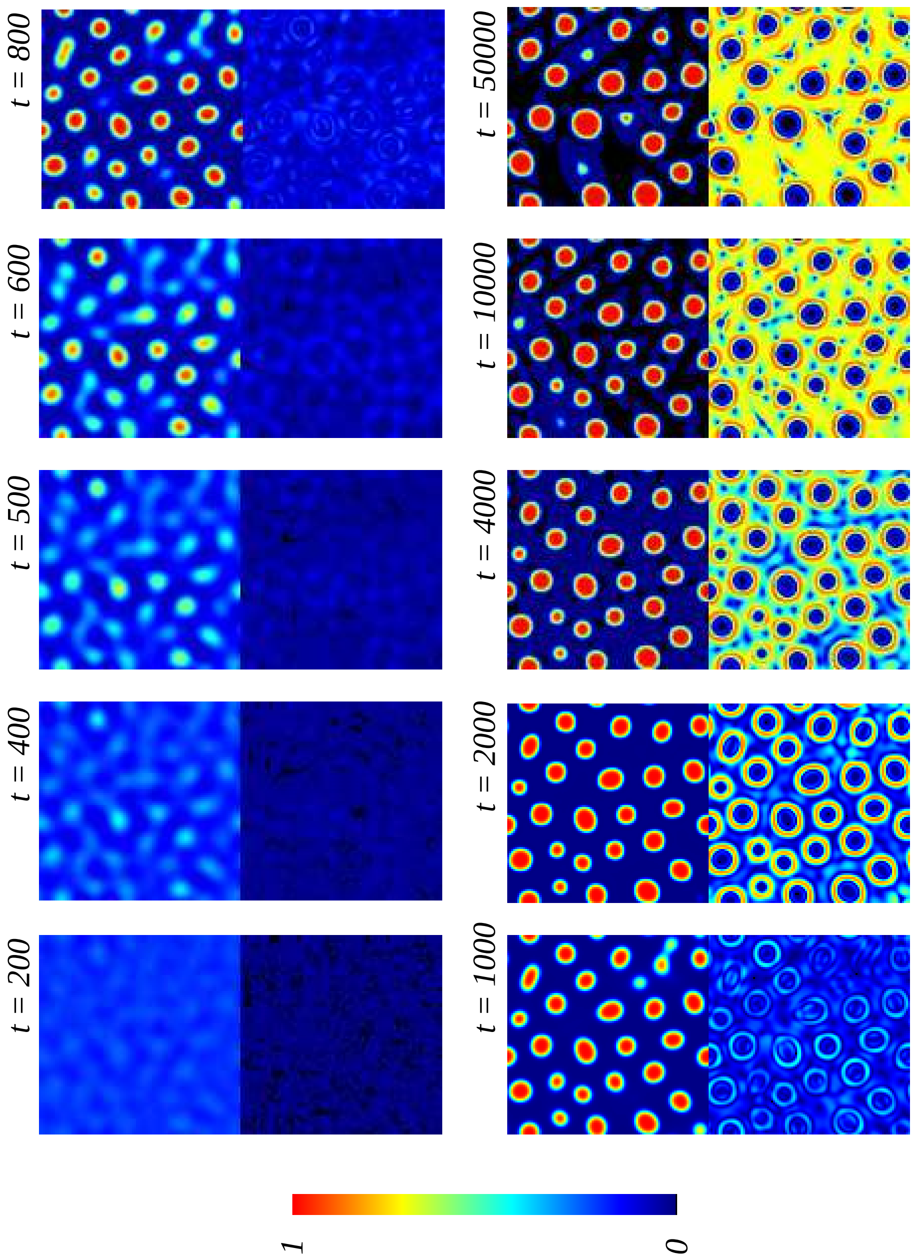

FIG. 15: Numerical simulations of the model for $L = 6$, $N = 6$, $\phi = 0.2$, $b = 2$, $\chi = 1.25$, $D_{||}L = 1$, $D_\phi = 0.1$, $D_r = 8.3 \times 10^{-4}$. The system is 150×150.